Molecular Therapy
Nucleic Acids
Original Article

Single intravitreal administration of a tetravalent siRNA exhibits robust and efficient gene silencing in mouse and pig photoreceptors

Shun-Yun Cheng,[1,2,3] Jillian Caiazzi,[4] Annabelle Biscans,[4] Julia F. Alterman,[4] Dimas Echeverria,[4] Nicholas McHugh,[4] Matthew Hassler,[4] Samson Jolly,[1] Delaney Giguere,[1] Joris Cipi,[1] Anastasia Khvorova,[4] and Claudio Punzo[1,2,3]

[1]Department of Ophthalmology and Visual Sciences, University of Massachusetts Chan Medical School, Worcester, MA 01605, USA; [2]Horae Gene Therapy Center, University of Massachusetts Chan Medical School, Worcester, MA 01605, USA; [3]Department of Neurobiology, University of Massachusetts Chan Medical School, Worcester, MA 01605, USA; [4]RNA Therapeutics Institute, University of Massachusetts Chan Medical School, Worcester, MA 01605, USA

Inherited retinal dystrophies caused by dominant mutations in photoreceptor (PR) cell expressed genes are a major cause of irreversible vision loss. Oligonucleotide therapy has been of interest in diseases that conventional medicine cannot target. In the early days, small interfering RNAs (siRNAs) were explored in clinical trials for retinal disorders with limited success due to a lack of stability and efficient cellular delivery. Thus, an unmet need exists to identify siRNA chemistry that targets PR cell expressed genes. Here, we evaluated 12 different fully chemically modified siRNA configurations, where the valency and conjugate structure were systematically altered. The impact on retinal distribution following intravitreal delivery was examined. We found that the increase in valency (tetravalent siRNA) supports the best PR accumulation. A single intravitreal administration induces multimonths efficacy in rodent and porcine retinas while demonstrating a good safety profile. The data suggest that this configuration can treat retinal diseases caused by PR cell expressed genes with 1–2 intravitreal injections per year.

INTRODUCTION

RNA interference is an endogenous molecular mechanism that uses small noncoding RNAs to regulate gene expression by mRNA silencing.[1] The discovery of small interfering RNAs (siRNAs) in gene regulation advanced the prospect of pharmacological approaches to treat diseases that conventional drug therapies cannot achieve.[2] During the early stages of siRNA therapy development, most oligonucleotide designs used naive and partially modified configurations.[3] However, clinical efficacy was limited due to major challenges in delivery, longevity, and safety of synthesized siRNAs.[4]

Full chemical stabilization of the siRNA scaffold was later introduced to increase the longevity of the siRNA in different tissues.[5] Biodegradability data of these fully stabilized scaffolds show a very favorable safety profile.[6,7] In addition to direct chemical modifications of siRNAs, covalent conjugations have also been explored to improve siRNA distributions in different organs.[4] Recent advancements with conjugated siRNAs have shown much more clinically relevant pharmacokinetics. Targeting liver diseases, siRNAs with a trimer of *N*-acetylgalactosamine (GalNAc) conjugate achieved efficient delivery by binding to the hepatocyte-specific asialoglycoprotein receptor, showing upwards of 6–12 months' effect in gene silencing with a single administration.[8–10] Although the platform is promising, with four clinically approved conjugated siRNAs for the liver,[11] its selectivity to liver hepatocytes limits its use in other organs. Previously, the hydrophobicity of conjugates has been shown to increase accumulation and efficacy in multiple extrahepatic tissue types.[12] Similarly, increasing the molecular size by generating multivalent configurations has also been shown to increase distribution and gene silencing in the brain[13] and lung.[14]

The first organ to be targeted by siRNA clinically was the eye.[15] Early on, nonmodified or partially modified siRNAs were used, resulting in limited efficacy and durability.[16] The eye is an ideal organ for siRNA treatment.[11] Its small and confined compartment allows lower drug doses to achieve a physiological improvement. In addition, the retina is immune privileged, and there are a multitude of dominant mutations that result in inherited retinal dystrophies (IRDs).[17] By far, the largest number of mutations affects genes expressed in the light-sensing rod photoreceptor (PR) cells. These mutations lead to IRDs, which are part of a family of mutations that cause retinitis pigmentosa.[17,18] Compared to recombinant adeno-associated virus (rAAV)–mediated gene transfer, the smaller size of the siRNA offers the potential advantage of treating many of these PR diseases by intravitreal delivery. This should result in a more uniform therapeutic outcome than what can be achieved by subretinal delivery of rAAV, which results only in local transduction around the injection bleb. Because there are several retinal cell types and different tissues within the eye (Figure S1), and the

Received 28 August 2023; accepted 30 November 2023;
https://doi.org/10.1016/j.omtn.2023.102088.

Correspondence: Anastasia Khvorova, PhD, RNA Therapeutics Institute, University of Massachusetts Chan Medical School, Worcester, MA 01605, USA.
E-mail: anastasia.khvorova@umassmed.edu
Correspondence: Claudio Punzo, PhD, Department of Ophthalmology and Visual Sciences, University of Massachusetts Chan Medical School, Worcester, MA 01605, USA.
E-mail: claudio.punzo@umassmed.edu

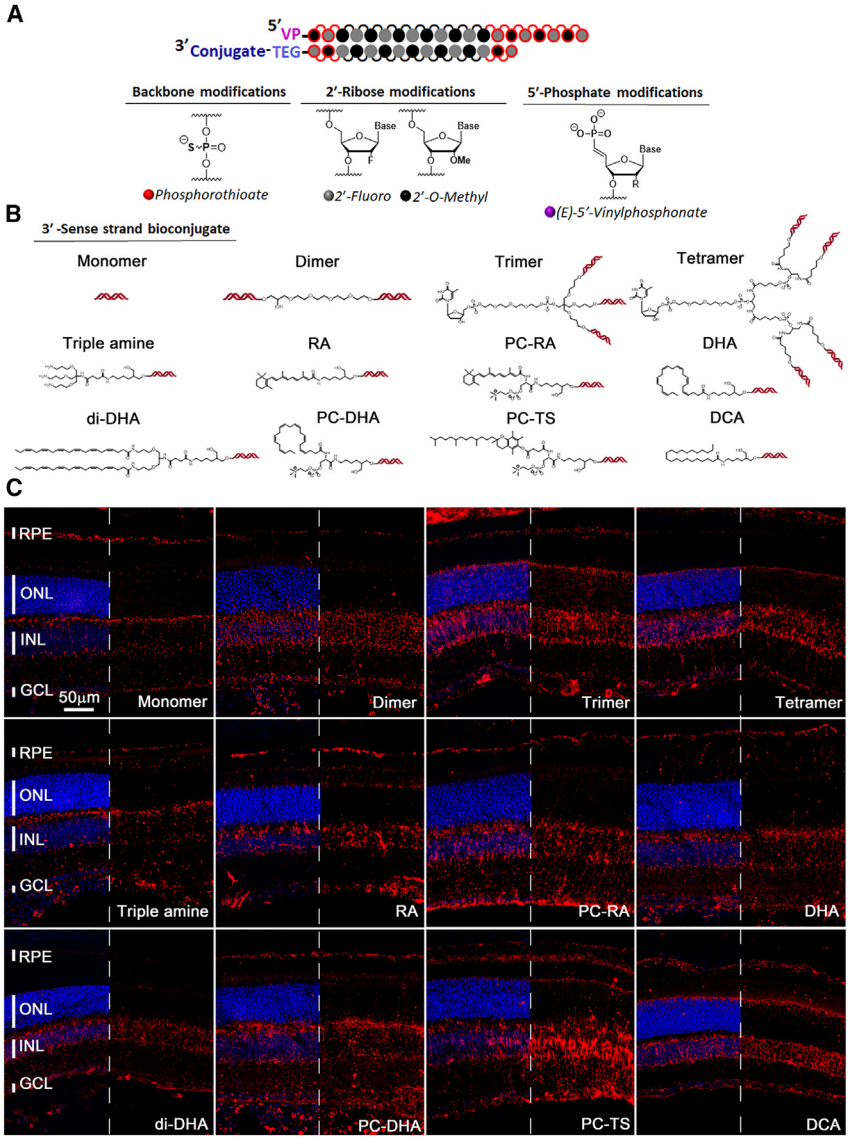

Figure 1. Distribution of different siRNA chemistries following intravitreal delivery

(A) Schematic of modifications on the siRNA backbone and ribose. (B) Schematics of the 12 configurations used, showing in the first row the structures of different valences and in rows 2–3 the structure of the conjugates. (C) Representative images of retinal cross-sections 3 days postintravitreal injection of 3 μg of siRNA per eye. Valency or conjugate is indicated in each panel in the same order as shown in (B). Blue: nuclei marked with DAPI, red: siRNAs labeled with Cy3. In each panel, half of the blue signal was removed to better visualize the red signal. Vertical bars indicate the height of different layers. Scale bar: 50 μm. Histology was repeated with at least N = 3 retinas.

structure of the conjugate and the siRNA have a profound impact on the tissue and cell distribution, we evaluated the impact of siRNA structures and conjugates on intraocular accumulation in different eye tissues and cell types, with a focus on PR cell enrichment. Recent work showed that conjugation of C16 to the siRNA supports efficient silencing in the retinal-pigmented epithelium (RPE) of the eye.[19] However, efficient gene silencing in retinal PR cells has not yet been evaluated systematically.

To identify bioconjugates and multivalent conformations that enrich in PR cells, we synthesized a panel of 12 fully chemically stabilized siRNA variants, all targeting the *Huntingtin* (*Htt*) gene,[20] where the nature of the hydrophobic conjugate or the valency was systematically altered.[12–14,20–22] We found that although most siRNAs variants distribute well throughout the retina, the tetravalent siRNA (hereafter referred as tetra-siRNA^{Htt}) exhibits the best enrichment in PR cells. Stability, safety, and silencing efficiency of tetra-siRNA^{Htt} were evaluated in both mouse and porcine retinas. In mice, a single intravitreal injection of 15 μg of the tetra-siRNA^{Htt} is sufficient to result in an ∼75% reduction in retinal HTT protein expression for up to 6 months. In pigs, in which eye size and vitreous volume are similar to those of humans, a single intravitreal injection of 300 μg of the tetra-siRNA^{Htt} results in a stable protein reduction of ∼80% for at least 4 months, which was the longest time point tested. Histological analyses of the retina did not reveal any long-term adverse immune reactivity in either animal model. The data suggest that therapeutically relevant gene silencing to treat PR cell–related retinal diseases is attainable with 1–2 intravitreal injections of chemically modified siRNA per year.

RESULTS

The structure and chemical configuration of the siRNA affects the distribution pattern in mouse retinas

Previous studies showed that hydrophobicity and multivalency can influence the pharmacokinetics and distribution of siRNAs.[13,14,20,23] To elucidate how different bioconjugates and valances affect siRNA distribution in the retina, we synthesized 12 chemical and structural siRNA variants.[12–14,20–22] The siRNAs were fully chemically modified, with a combination of 2′-*O*-methylation (2′-OMe), 2'-fluoro (2′-F), vinylphosphonate, and phosphorothioates (Figure 1A). All of the compounds targeted the *Htt* gene and tagged with a Cy3 fluorophore for visualization.[20,22] *Htt* was used as a target because it is ubiquitously expressed, and the targeting sequence has been previously validated across different species and assays in combination with the chemistries tested here.[20,22] We have previously established that the Cy3 dye does not principally contribute to the cellular distribution in the context of these configurations.[24] The modified chemical architectures tested included four different valences, monovalent,[14] divalent,[13,14] trivalent,[14] and tetravalent,[14] as well as different conjugates, such as triple-amine,[22] retinoic

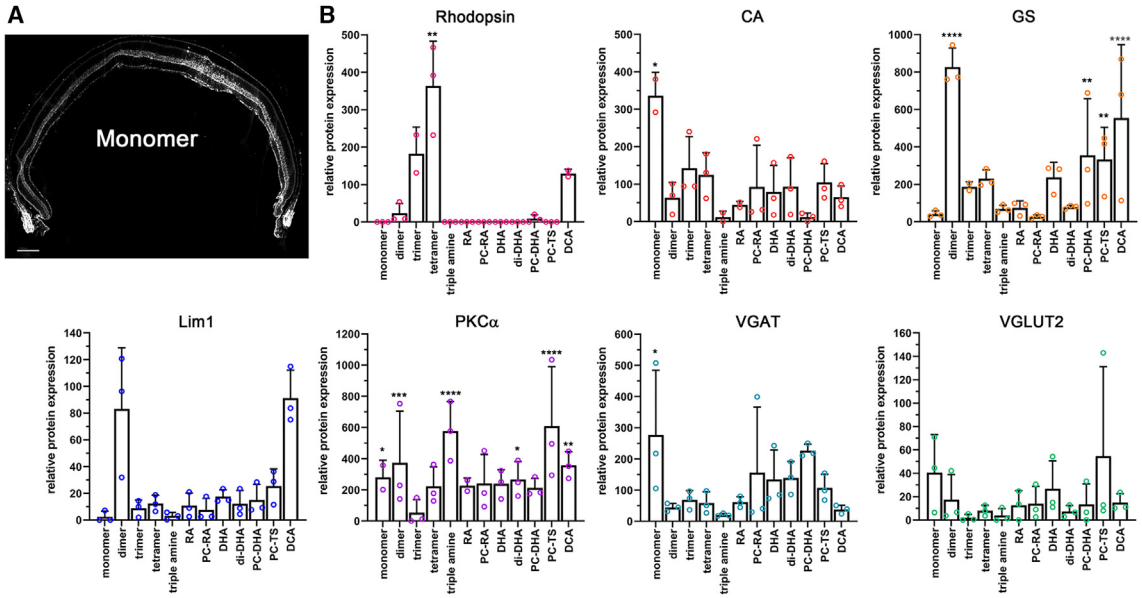

Figure 2. Enrichment of siRNA chemistries in different retinal cell types

(A) Cross-section showing efficient distribution of monomer siRNA labeled with Cy3 across entire retinal cross-section. Image shown in grayscale to better visualize the Cy3 signal. (B) Western blot quantifications with cell type–specific antibodies from protein extracts of FACS cells that were $Cy3^{+}$. The y axis shows relative enrichment in percentage when compared to total protein extracts from an uninjected retina. Antibodies: rhodopsin (rod PR cells), CA (cone PR cells), GS (Müller glia cells), Lim1 (mainly horizontal cells), PKCα (mainly rod bipolar cells), VGAT (amacrine cells, horizontal cells), and VGLUT2 (ganglion cells). A multiple t test was performed to determine significance with uninjected total retinal extracts. N = 3 samples; error bars: SD. *$p < 0.05$; **$p < 0.01$; ***$p < 0.001$; ****$p < 0.0001$.

acid (RA),[22] PC-RA (phosphocholine-RA),[22] docosahexaenoic acid (DHA),[21,22] di-docosahexaenoic acid (di-DHA),[23] phosphocholine-docosahexaenoic acid (PC-DHA),[22] phosphocholine-α-tocopheryl succinate (PC-TS),[22] and docosanoic acid (DCA)[22,25] (Figure 1B). Adult mice were injected intravitreally with 1 μL of each siRNA (3 μg/μL), and tissues were collected 3 days postinjection for section analyses. We found a predominant enrichment of siRNAs in the inner nuclear layer (INL) region, reminiscent of a Müller glia cell pattern and where most cells are bipolar and amacrine cells (Figure S1), with all conjugates and valances (Figure 1C), and a relative uniform distribution of the siRNA across the entire retina (Figure 2A). Most also showed accumulation in the ganglion cell layer (GCL) and in the RPE (Figure 1C). Accumulation in PR cells seemed to occur preferentially with the trimer, tetramer, and DCA, based on the signal seen in the outer nuclear layer (ONL) and PR cell inner segment (IS) region. Like previous observations in the mouse brain,[13] the unconjugated monomer displayed the least siRNA retention in the retina. Nevertheless, the Cy3 signal seen seemed to show spotty accumulation in the outer plexiform layer and where PR cell ISs reside, at an interval consistent with cone PR cell pedicles and cone ISs, respectively (Figure 1C).

To better identify the cell types in which the different siRNAs enrich, we repeated the injections, dissociated the retinas 3 days postinjection, and collected Cy3-labeled cells by fluorescence-activated cell sorting (FACS). Cell type–specific antibodies were then used to determine by western blot which cell types are enriched by each chemistry (Figure 2B). To capture most of the retinal cell types, we used antibodies against rhodopsin (rod PR cells), cone arrestin (CA; cone PR cells); glutamine synthetase (GS; Müller glia cells), LIM class homeodomain transcription factor (Lim1[26]; horizontal cells), protein kinase Cα (PKCα[27]; rod bipolar cells), vesicular GABA transporter (VGAT[28]; amacrine cells, horizontal cells), and vesicular glutamate transporter 2 (VGLUT2[29]; ganglion cells, Müller glial cells). Statistically significant enrichments were seen for rods, cones, Müller glia, bipolar cells, and amacrine cells. As predicted by the histological analyses (Figure 1C), the multivalent chemistry and DCA were very efficient for siRNA enrichment in PR cells (monovalent for cones and tetravalent for rods). The strongest enrichment in Müller glia cells was seen with the divalent chemistry. Bipolar cells and amacrine cells also showed an enrichment with most chemistries because combined they account for ∼80% of all INL cells. Surprisingly, most lipid modifications did not enhance uptake into rod PR cells, although rods are rich in lipids, in particular, DHA. Thus, similar to systemic, CNS, and lung delivery, the structure and chemical composition of the siRNA has a profound impact on the intraretinal distribution profile, indicating that different conjugates may be optimal for different cell types. Because the tetravalent configuration displayed the strongest enrichment in rod PR cells and still enters cone PR cells, it was selected for the detailed examination of safety, distribution, and functional silencing efficiency.

Tetrameric siRNA displays a dose-dependent, safe, and long-term silencing effect of HTT in mouse retinas

We evaluated the efficacy of the tetra-$siRNA^{Htt}$ at different dose levels in mice eyes. Mice were injected intravitreally with 2 μL of tetra-$siRNA^{Htt}$

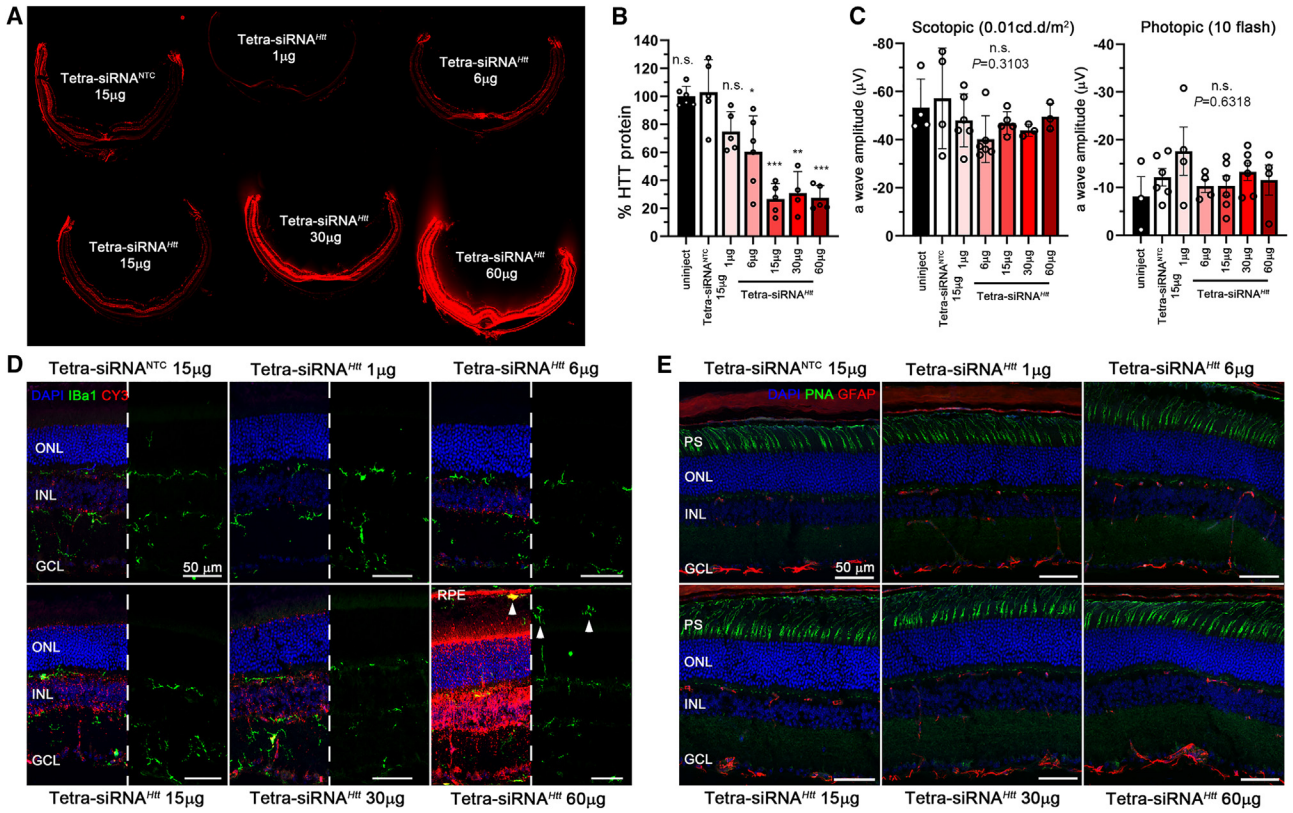

Figure 3. Dose escalation of tetra-siRNA^{Htt} in mouse

(A) Retinal cross-sections of mice 2 months postinjection of 2 µL siRNA (doses indicated in each individual section shown in panel). Seen is the siRNA distribution through the fluorescence of the attached Cy3 fluorophore. (B) Dose response at 2 months postinjection using the same doses and injection volume as shown in (A). Shown is the percentage of the remaining HTT protein compared to the NTC. (C) Scotopic (first graph) and photopic (second graph) a-wave amplitudes from ERG recordings at 2 months postinjection. N = 6 for (A)–(C); error bars: SD; significance is compared to NTC; n.s., not significant. *p < 0.05; **p < 0.01; ***p < 0.001. (D and E) Retinal cross-sections shown in (A) stained for Iba1 (D: green signal) and GFAP (E: red signal) to visualize migrating microglia and activation of gliosis, respectively. Except for the highest dose (60 µg), there are no microglia (white arrowheads) seen in the ONL or where PR cell segments reside. Blue: nuclei marked with DAPI; green: Iba1 in (D) and peanut agglutinin lectin (PNA) marking cone PR cell segments in (E); red: siRNA in (D) marked through Cy3 label and GFAP in (E). In each part of (D), half of the blue and red signal was removed to better visualize the green signal. Histology in (A), (D), and (E) was repeated with at least N = 3 retinas. PS, photoreceptor segments. White arrowheads mark microglia in the subretinal space; vertical bars indicate height of different layers. Scale bars: 50 µm.

to accommodate dose ranges of 1, 6, 15, 30, and 60 µg per eye. Histological analyses at 2 months postinjection revealed a uniform distribution of the Cy3-labeled siRNA, with a signal intensity proportional to the injected dose (Figure 3A). Gene silencing by the previously optimized *Htt* sequence[20] was evaluated by western blot. We found a dose-dependent reduction in HTT protein (Figure 3B), with a statistically significant difference in gene silencing when compared to the nontargeting control (NTC) starting at 6 µg of tetra-siRNA^{Htt}. The silencing efficiency started to plateau at ~15 µg of tetra-siRNA^{Htt} because higher doses did not lead to more reduction in HTT protein. The gene silencing efficiency of the plateau was ~70% when compared to the NTC-injected eyes. The NTC, which consists of a scrambled sequence of the same chemical configuration,[20] showed no reduction in HTT protein at the plateau dose of 15 µg when compared to uninjected animals, indicating the specificity of the observed silencing activity (Figure 3B).

To evaluate safety, we performed electroretinogram (ERG) recordings under scotopic (rod PR cell response) and photopic (cone PR cell response) conditions, which revealed no significant differences among the different dose groups (Figures 3C and S2). Similarly, immunohistochemical analyses of retinal cross-sections detected no migration of microglia marked by ionized calcium binding adaptor molecule 1 (Iba1) into the ONL and/or inner outer segment region, except for occasional cells at the highest dose (60 µg; arrowheads, Figure 3D). Consistent with this, there was no reactive gliosis in the retina as assessed by the normal expression of glial fibrillary acidic protein (GFAP) (Figure 3E). Both Iba1 and GFAP are markers that assess early retinal immune responses and early signs of neurodegeneration.[30] Together, the data indicate an efficient and safe gene silencing by the tetra-siRNA^{Htt} in the mouse retina.

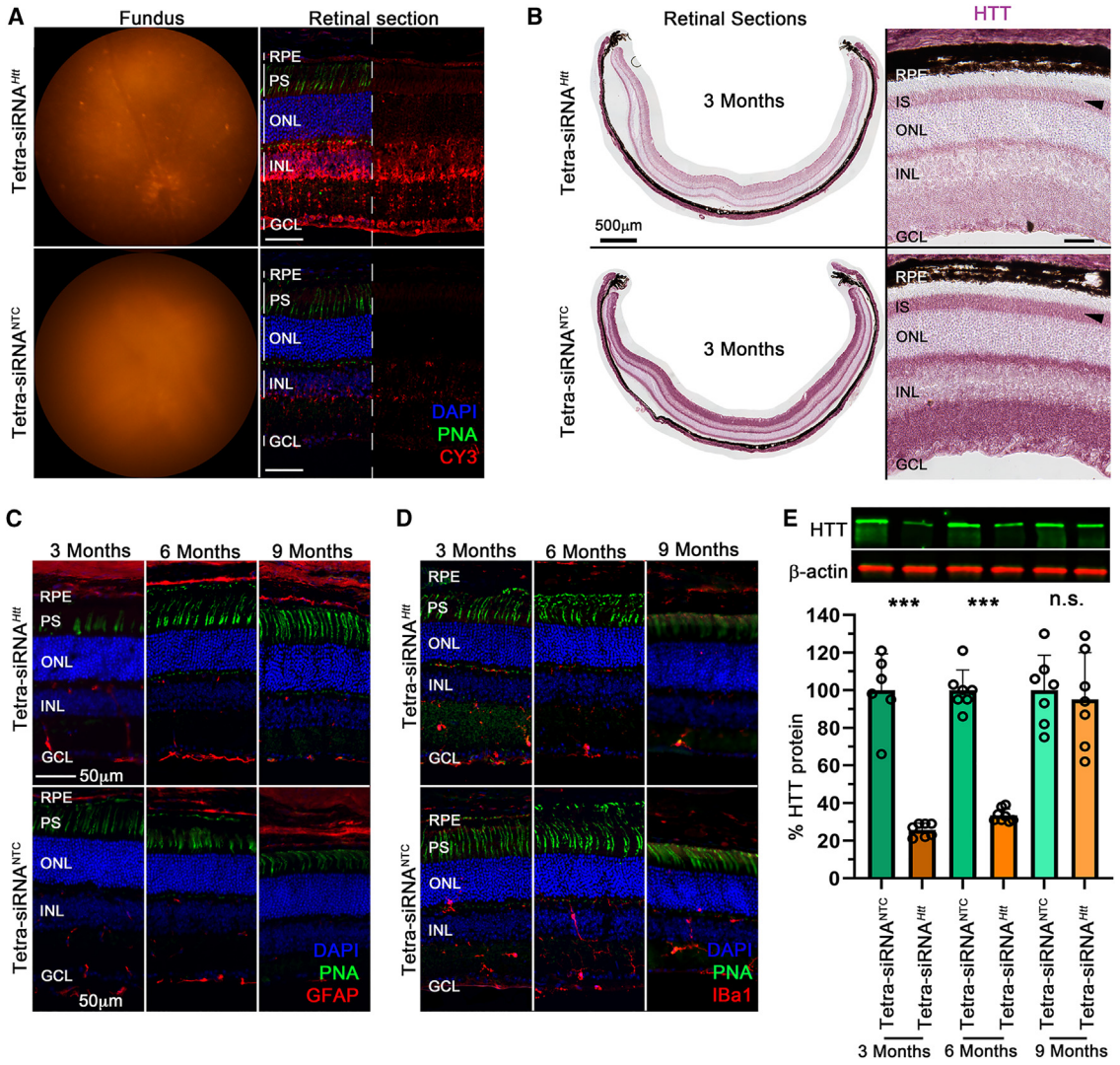

Figure 4. Long-term silencing of HTT with tetra-siRNA^{Htt}

(A) Fluorescent fundus images and retinal cross-section of mice injected with 15 μg of the tetra-siRNA^{Htt} and the tetra-siRNA^{NTC} imaged at 3 months postinjection. (B) Retinal cross-sections at 3 months postinjection stained for expression of the HTT protein (purple signal). Shown is an entire cross-section (left) and a magnified view (right). Reduction of HTT protein in PR cell ISs is indicated by black arrowheads. (C and D) Retinal cross-sections stained for GFAP (red signal) and Iba1 (red signal) at 3, 6, and 9 months postintravitreal injection of 15 μg siRNAs to visualize the activation of gliosis and migration of microglia, respectively. (E) Quantification of remaining retinal HTT protein over time after 1 intravitreal injection of 15 μg siRNAs. Top shows example of protein bands on western blot and bottom shows quantification. Shown is the percentage of remaining HTT protein compared to the NTC for each time point. N = 6–7 retinas per time point and siRNA type; error bars: SD. ***$p < 0.001$. (A, C, and D) Blue: nuclei marked with DAPI; green: cone segments marked with peanut agglutinin lectin (PNA); red: siRNAs in (A) marked by Cy3 label and GFAP, and by Iba1 in (C) and (D). In (A), half of the blue and green was removed to better visualize the red signal. Scale bars: 50 μm, except in (B), as indicated. Histology in (A)–(D) was repeated with at least N = 3 retinas.

To examine the longevity of tetra-siRNA^{Htt}, mice were intravitreally administered a medium dose (15 μg/eye) of tetra-siRNA^{Htt}, and silencing efficiency was evaluated at 3, 6, and 9 months postinjection. The tetra-siRNA^{NTC} was used as a control. At 3 months postinjection, the tetra-siRNA^{Htt} was easily visualized by fluorescent funduscopy and fluorescent microscopy on retinal cross-sections (Figure 4A). Section analyses for HTT protein expression showed a strong reduction of HTT protein throughout the retina, including PR-ISs, showing that the tetra-siRNA^{Htt} does target PR cells efficiently (Figure 4B). Similar to the dose escalation study, in which there was no inflammation at 2 months postinjection with a dose of 15 μg, there was no change in GFAP (Figure 4C) and Iba1 (Figure 4D) expression at all 3 time points. Western blot quantification of HTT protein showed a robust reduction of ∼75% and ∼70% of HTT protein at 3 and 6 months postinjection, respectively. However, by 9 months postinjection, there were no significant differences between the two groups

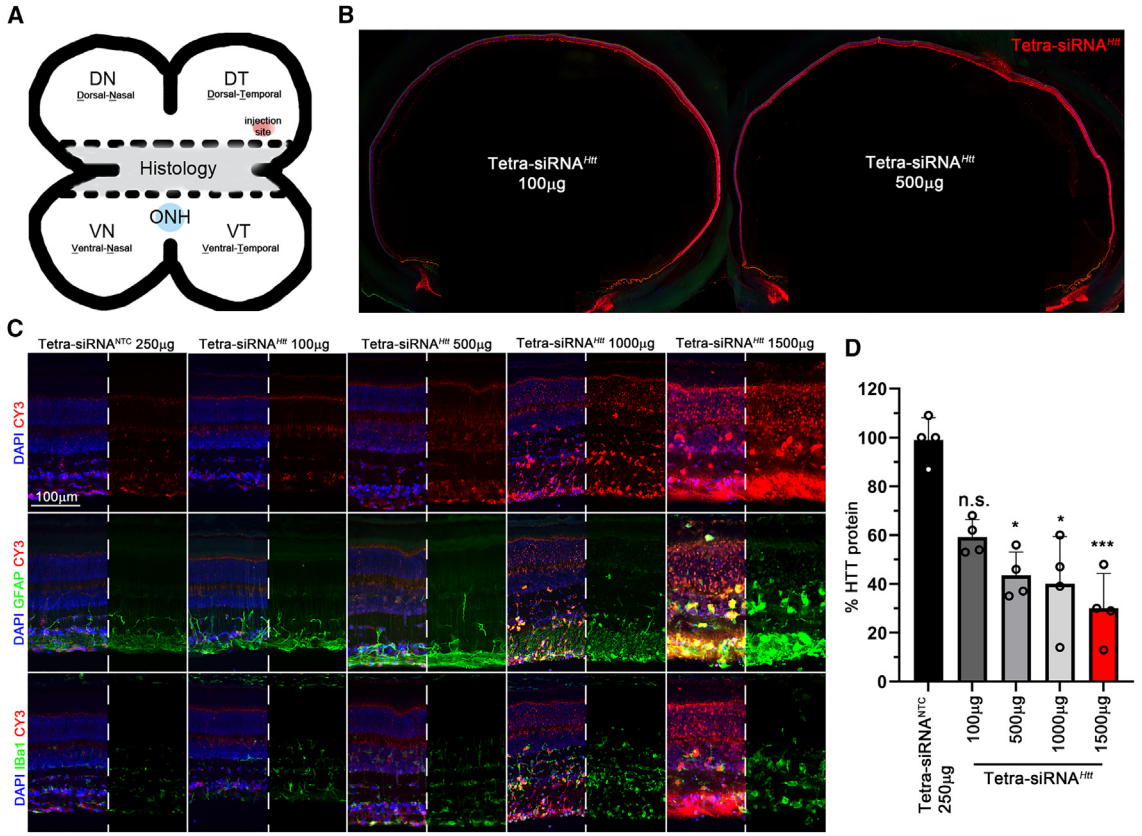

Figure 5. Dose escalation of tetra-siRNA^{Htt} in porcine eyes

(A) Schematic of how porcine eyes were processed and where eyes were injected. The central part was used for histological analyses and the dorsal and ventral parts of the eye were used for quantitative analyses. ONH, optic nerve head. (B) Distribution of Cy3-labeled siRNA across the eye 14 days postintravitreal injection at doses indicated. (C) Retinal cross-section of eyes 14 days postintravitreal injection with siRNAs. Doses are indicated on the top of each column. Sections were stained for GFAP (center row) or Iba1 (bottom row) to visualize activation of gliosis and migration of microglia, respectively. Blue: nuclei marked with DAPI; green: GFAP or Iba1 as indicated; red: siRNAs marked by Cy3 label. In each panel, half of the blue signal and for rows 2 and 3 the red signal were removed to better visualize the green signal in rows 2 and 3 and the red signal in row 1. Scale bar: 100 µm. (D) Percentage quantification of remaining retinal HTT protein when compared to NTC at 14 days postintravitreal injection at doses indicated in the bar graph. Each quantification represents the average of the 4 quadrants of 1 eye. Error bars: SD; significance is compared to NTC. *$p < 0.05$; ***$p < 0.001$.

(Figure 4E). In summary, the mouse data indicate that PR cell expressed genes can be efficiently downregulated with the tetra-siRNA^{Htt} in a safe manner over a prolonged period of time.

Tetra-siRNA^{HTT} delivery in porcine retina

In mouse, the lens is ∼20% larger than the vitreous, which is in contrast to the human anatomy, in which the lens volume is ∼16 times smaller than the vitreous volume. In addition, the human vitreous is ∼500 times larger than the mouse vitreous. These differences in relative and absolute sizes may alter how siRNAs behave in large eyes. To test the suitability of the tetra-siRNA^{Htt} for clinical use, we injected the tetra-siRNA^{Htt} intravitreally into the dorsal-temporal sclera (Figure 5A) of porcine eyes.[31] An initial dose escalation (100, 500, 1,000, and 1,500 µg) was used to determine distribution, toxicity, and silencing efficiency over a period of 2 weeks (Figures 5B–5D). Upon enucleation the cone-dominant central visual streak was processed for histology (Figure 5A), and the remaining peripheral quadrants (Figure 5A) were used to quantify the silencing of HTT protein (Figure 5D). Distribution of the Cy3-labeled tetra-siRNA^{Htt} appeared to be dose and injection site dependent (Figure 5B), which was confirmed by western blot analyses of the four quadrants within one eye (Figure 5D). The average silencing efficiency increased by only ∼10% between 500 (∼60% silencing) and 1,500 µg (∼70% silencing), suggesting a possible saturation at ∼500 µg/eye. Histological analyses revealed an increase in GFAP expression and Iba1^{+} microglia starting at 1,000 µg/eye, indicating that the higher doses cause retinal toxicity (Figure 5C). At 500 µg/eye, only a moderate upregulation of GFAP in Müller glial and no migration of microglia into the ONL were seen, suggesting that doses below 500 µg/eye are safe for large eyes.

To assess silencing efficiency and toxicity over time, we injected a dose deemed safe from the dose escalation study (300 µg/eye) and analyzed the tissue at 1 and 4 months postinjection. Histological

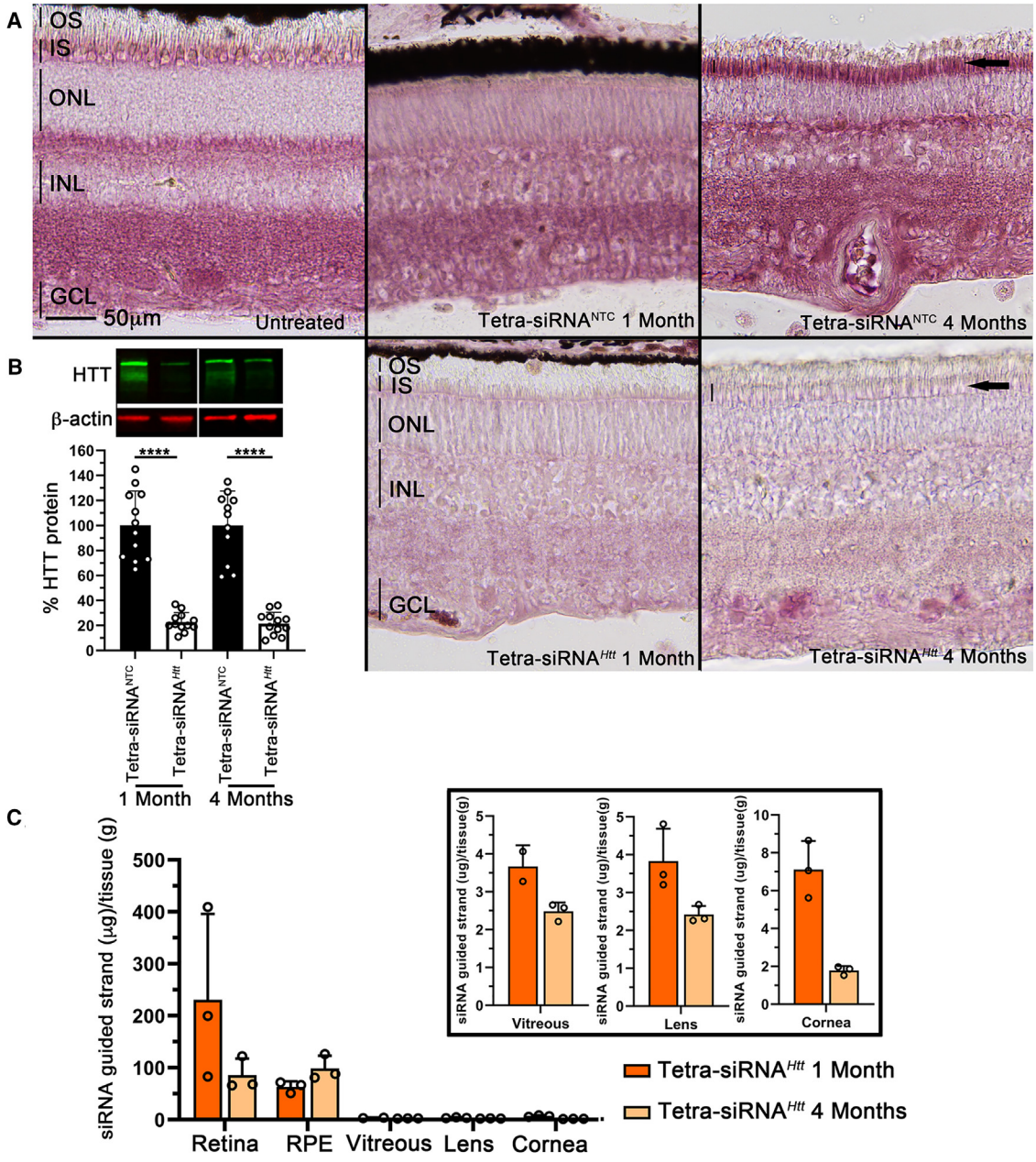

Figure 6. Long-term HTT silencing with tetra-siRNA^{Htt} in porcine retina

(A) Retinal cross-section stained for expression of the HTT protein (purple signal). Top row shows uninjected or NTC-injected eyes at 1 and 4 months postinjection with 300 μg of siRNA. Bottom row shows tetra-siRNA^{Htt}-injected eyes with same dose. Silencing in PR ISs (arrows and vertical bars marking height of IS in last column) is still clearly visible at 4 months postinjection. Images are representative images from 3 pigs per time point and siRNA. Scale bar: 50 μm. (B) Percentage quantification of remaining retinal HTT protein at 1 and 4 months postinjection when compared to the NTC. Top image shows examples of bands on western blot gel. Quantification represents the average of the 4 quadrants of 3 eyes. N = 12; error bars: SD. ****p < 0.0001. (C) Pharmacokinetics of remaining siRNA in different eye tissues at 1 and 4 months postinjection. A PNA hybridization assay was performed with 1 quadrant per eye. N = 3, error bars: SD. Analyses of the retina, RPE, vitreous, lens, and cornea show that most of the siRNA is taken up by the retina and RPE and is cleared from the vitreous. In addition, very little migrates to the lens and cornea. Eye tissues from NTC-injected eyes did not show any signal and were therefore omitted from the figure. Boxed area shows vitreous, lens, and cornea graphs with adjusted y scales.

analyses showed a clear reduction of HTT protein that was maintained over a period of 4 months (Figure 6A). In particular, the reduction in PR-ISs was clearly visible (Figure 6A, arrows). The histological data were corroborated by western blot analyses, which showed an ~80% reduction in HTT protein over the duration of the 4 months (Figure 6B). To understand the pharmacokinetics of

the siRNA, we measured its distribution within the different tissues of the eye by performing a peptide nucleic acid (PNA) hybridization assay[32] at 1 and 4 months postinjection (Figure 6C). The PNA assay evaluates the presence of the guide strand, which is not dependent on the presence of the fluorescent label. The highest concentration of siRNA was found in the retina, followed by the RPE. The vitreous, cornea, and lens had detectable amounts of the oligonucleotide, which was at least 50-fold lower (Figure 6C). Interestingly, in the RPE, the concentration of the siRNA remained stable between 1 and 4 months postinjection, whereas it declined in all of the other tissues. Finally, analyses of Iba1 and GFAP expression revealed few microglia migrating into the subretinal space close to the injection site at 1 month postinjection; however, this transient migration was not observed at 4 months postinjection (Figure S3A). Similarly, there was mild gliosis near the injection site at 1 month but not at 4 months postinjection, as seen in the changes in GFAP expression (Figure S3B). In summary, the data suggest that safe, efficient, and long-lasting silencing of PR cell expressed genes is feasible as a therapy in humans with tetra-siRNA^{Htt}s.

DISCUSSION

Here, we examined 12 different modified siRNAs and their retinal cell distribution. We show that although all of them distribute well across the retina, the nature of the siRNA structure and the conjugate has a significant impact on the preference of the cellular distribution. One interesting finding was that none of the lipid conjugates showed any preferential enrichment in PR cells. In contrast, the tetra-siRNA^{Htt} did show PR cell enrichment and was therefore evaluated further for silencing efficiency, safety, and longevity in mouse and porcine retinas. The histological analyses in mouse and porcine showed that the tetra-siRNA^{Htt} is quite effective at causing HTT silencing in PR cells. In the mouse, the silencing appears to last between 6 and 9 months. Although we did not determine the silencing duration in porcine retinas past 4 months, it is safe to assume from the data collected that a similar if not longer time window applies to the porcine retina. This is therapeutically relevant because depending on the disease that is being treated, 1–2 intravitreal injections per year may be sufficient for a significant therapeutic effect. Many IRD-related genes are associated with dominant mutations in PR cell expressed genes, meaning that silencing the mutated copy of the gene may be sufficient to significantly delay disease progression. siRNAs represent an ideal approach for this type of mutation. The most significant advantage of the siRNA approach over the rAAV approach in targeting PR cells is the intravitreal delivery route. Although it is less risky and invasive, it also results in widespread targeting of all PR cells. This is likely to result in a better therapeutic outcome over time, when compared to the local PR transduction that is achieved with rAAVs. In addition, once a chemistry is selected and tested for safety, the only changes needed to treat a different dominant IRD are changes in a few nucleotides of the siRNA sequence. This can significantly increase the speed and decrease the cost at which therapies can be developed, making eye-saving injections available to the many who still suffer from these debilitating diseases.

Many non-IRDs such as diabetic retinopathy, diabetic macular edema, and the exudative form of age-related macular degeneration (AMD) could also benefit from long-lasting siRNA therapies. All of these diseases are caused by abnormal neovascularization. Currently, these diseases are treated with anti-vascular endothelial growth factor (VEGF) inhibitors requiring intravitreal injections at a frequency of every 4–8 weeks.[33] To date, there are two clinical trials using siRNA to treat these diseases[34–37]; however, these trials were stopped due to a failure to reach the primary endpoint. Our divalent chemistry enriched well in Müller glia cells and to some extent in the RPE. Both cell types are believed to be important cells to be targeted to reduce retinal VEGF levels in these diseases.[38] Similarly, a new US Food and Drug Administration–approved drug that delays disease progression in the dry form of AMD targets the complement system in RPE cells,[39,40] with an injection frequency of every 4–8 weeks. The frequency of injections for these age-related illnesses is a burden to elderly patients. Any therapeutic approach that reduces the intraocular injection frequency constitutes a significant improvement in the quality of life for these patients. In summary, by taking a cell type–specific approach, we have identified chemistries for the efficient transduction of Müller glia cells and PR cells. These chemistries represent new opportunities for how age-related retinal diseases as well as IRDs can be treated in the future. In addition, they increase speed and reduce costs for the development of these sight-saving treatments.

MATERIALS AND METHODS

Animals

All of the procedures involving animals were in compliance with the Association for Research in Vision and Ophthalmology Statement for the Use of Animals in Ophthalmic and Vision Research and were approved by the Institutional Animal Care and Use Committees of the University of Massachusetts Medical School. The mice used in the study were between the ages of 2 and 3 months at the time of injection and were C57BL/6J mice purchased from The Jackson Laboratory. The pigs used in the study were between the ages of 1 and 2 months at the time of injection and were Yorkshire pigs purchased from Earl Parsons and Sons.

Oligonucleotide synthesis

Oligonucleotides were synthesized by phosphoramidite solid-phase synthesis on a MerMade12 (Biosearch Technologies, Novato, CA) or on AKTA Oligopilot 10 or 100 (Cytiva, Marlborough, MA) using 2'-F- or 2'-OMe-modified phosphoramidites with standard protecting groups. 5′-(E)-Vinyltetraphosphonate (pivaloyloxymethyl) 2′-*O*-methyluridine 3′-cyanoethyl (CE) phosphoramidite (VP) was purchased from Hongene Biotech (Union City, CA), Cy3 phosphoramidite (Quasar 570 CE) was used to label the oligonucleotides purchased from GenePharma (Shanghai, China). Trivalent and tetravalent oligonucleotides were prepared using commercial trebler and doubler phosphoramidites, respectively, as branching points (Glen Research, Sterling, VA) and tetraethyloxy-glycol phosphoramidite (TEG) (ChemGenes, Wilmington, MA) as spacer from the solid support. Phosphoramidites were prepared at 0.1 M in anhydrous acetonitrile (ACN), except for 2′-*O*-methyl-uridine phosphoramidite

dissolved in anhydrous ACN containing 15% dimethylformamide. 5-(Benzylthio)-^{1}H-tetrazole was used as the activator at 0.25 M, and the coupling time for all phosphoramidites was 4 min, except for trebler, doubler, and TEG phosphoramidites, where the coupling time used was 8 min. Detritylations were performed using 3% trichloroacetic acid in dichloromethane (MerMade12) or in toluene (AKTA). The capping reagents used were CAP A (20% *n*-methylimidazole in ACN) and CAP B (20% acetic anhydride and 30% 2,6-lutidine in ACN). Phosphite oxidation to convert to phosphate or phosphorothioate was performed with 0.05 M iodine in pyridine-H_2O (9:1, v/v) or 0.1 M solution of 3-[(dimethylaminomethylene)amino]-^{3}H-1,2,4-dithiazole-5-thione in pyridine (ChemGenes) for 3 min. Reagents for detritylation, iodine oxidation, and capping were purchased from AIC, Westborough, MA. Unconjugated oligonucleotides were synthesized on 500 Å (or 1,000 Å for trivalent and tetravalent oligonucleotides) long-chain alkyl amine (LCAA) controlled pore glass (CPG) functionalized with UnyLinker terminus (ChemGenes). Divalent oligonucleotides were synthesized on modified solid support prepared in-house.[13] DCA, DHA, RA, PC-DHA, PC-RA, PC-TS, di-DHA, and triple amine, bioconjugated oligonucleotides were synthesized on modified solid supports prepared in-house.[21–23]

Deprotection and purification of oligonucleotides for *in vivo* experiments

Cy3 labeled bioconjugated oligonucleotides were cleaved and deprotected in 28%–30% ammonium hydroxide-40% aqueous methylamine (1:1, v/v) (AMA) for 2 h at room temperature. Cy3 labeled multivalency oligonucleotides (monovalent, divalent, trivalent, and tetravalent) were cleaved and deprotected by AMA treatment for 2 h at 45°C. The VP containing oligonucleotides was cleaved and deprotected as described previously.[41] Briefly, CPG containing VP-oligonucleotides was treated with a solution of 3% diethylamine in 28%–30% ammonium hydroxide at 35°C for 20 h. All of the solutions containing cleaved oligonucleotides were filtered to remove the CPG and dried under vacuum. The resulting pellets were resuspended in 5% ACN in water. Purifications were performed on an Agilent 1290 Infinity II HPLC system (Agilent Technologies, Santa Clara, CA). VP-oligonucleotides were purified using a custom 20 × 150-mm column packed with Source 15Q anion exchange resin (Cytiva); running conditions: eluent A, 10 mM sodium acetate in 20% ACN in water; eluent B, 1 M sodium perchlorate in 20% ACN in water; and linear gradient, 10%–35% eluent B in 40 min at 50°C. Cy3 labeled multivalency and bioconjugated oligonucleotides were purified using a 21.2 × 150-mm PRP-C18 column (Hamilton Company, Reno, NV); running conditions: eluent A, 50 mM sodium acetate in 5% ACN in water; eluent B, 100% ACN; linear gradient, varied due to hydrophobicity differences of the bioconjugates in the range 10%–70% eluent B in 40 min at 60°C. The flow was 30 mL/min in both methods, and peaks were monitored at 260 nm for nonlabeled oligonucleotides and 550 nm for Cy3 labeled oligonucleotides. Fractions were analyzed by liquid chromatography-mass spectrometry, and pure fractions were combined and dried under vacuum. Pure oligonucleotides were resuspended in 5% ACN and desalted by size exclusion on 25 × 250-mm custom columns packed with Sephadex G-25 media (Cytiva); separate columns were used for nonlabeled and Cy3 labeled oligonucleotides. Desalted oligonucleotides were finally lyophilized.

PNA hybridization assay

siRNA accumulation was quantified as described previously using PNA hybridization assay.[32] Harvested pig eye tissue was weighed and lysed in 300 μL homogenizing buffer (no. 10642, Affymetrix, Santa Clara, CA) using a Qiagen TissueLyser II (Qiagen, Germantown, MD) except for cornea, which was lysed in 1 mL using the Bio-Gen PRO200 Homogenizer (01-01200, PRO Scientific, Oxford, CT).

Cell collection using flow cytometry

Retinas from two injected mice for each of the different Cy3-labeled siRNAs were pooled and dissociated into single cells using papain for dissociation according to the manufacturer's instructions (catalog no. 9035-81-1, Worthington Biochemical, Freehold, NJ). Each conjugate was done in triplicate, with a total of 6 mice per configuration. $Cy3^{+}$ cells were collected by FACS for western blot analysis to measure which modification enriched for which cell type–specific protein.

Intravitreal administration of siRNAs in mice and swine

Intravitreal injections in mice were performed as previously described.[42] The same glass needles (catalog no. B100-58-50, Clunbury Scientific, Bloomfield Hills, MI) were used in combination with the FemtoJet (Eppendorf, Framingham, MA) with a constant pressure and time to deliver ∼1–2 μL of siRNA into the vitreous. Depending on the experiment, various amounts of siRNA were used as noted in the text. Intravitreal injections in pigs were done under anesthesia, which was performed and supervised by Animal Medicine at the University of Massachusetts Chan Medical School. After the pigs were fully anesthetized, proparacaine and iodine were used to numb and disinfect the eye, respectively. A sterile insulin syringe was used to deliver 100 μL of siRNA into each eye. The injection sites were always ∼2–3 mm away from the limbus on the temporal side of the eye. The injection was performed like an intravitreal injection for anti-VEGF drugs. After injection, sterile saline was used to rinse the eye. Injected amounts are described in the text.

Funduscopy and electroretinography

Funduscopy was performed as previously described.[43] In addition to regular bright-field visualization, the TRITC filter was used to visualize the retention of the Cy3-labeled siRNAs in the retinas. Images were acquired with the Micron IV System from the Phoenix Technology Group (Lakewood, CO). ERGs were performed as previously described[43] in mice that were injected with the doses indicated in Figure 2C, at 2 months postinjection. ERGs were performed with the Celeris System (Diagnosys, Lowell, MA) and their preset programs for scotopic and photopic recordings. The data shown represent the average of 6–7 mice and were recorded with the following parameters: scotopic recordings were performed at 1 cd · s/m^2, and photopic ERG recordings used a background intensity of 9 cd · s/m^2 and a flash intensity of 10 cd · s/m^2.

Histology

Mouse retinal dissection, histological preparation, and immunohistochemistry staining procedures were performed as previously described.[43] The following antibodies were used: HTT (1:300; catalog no. 5656, Cell Signaling Technology, Danvers, MA), fluorescein peanut agglutinin lectin (PNA) (1:1,000; catalog no. FL1071, Vector Laboratories, Newark, CA), rabbit anti-Iba1 (1:300; catalog no. 019–19741, Wako Chemicals, Richmond, VA), mouse anti-GFAP (1:1,000; catalog no. MAB5628, Millipore, Burlington, MA), and rhodamine phalloidin (1:1,000; catalog no. R415, Life Technologies, Carlsbad, CA). Nuclei were counterstained with 4′,6-diamidino-2-phenylindole (DAPI) (catalog no. 9542, Sigma-Aldrich, St. Louis, MO). siRNAs were visualized by their Cy3 signal without signal enhancement. Porcine histological procedures used the same method as that for mice with the following modification. From each eye, a ∼10-mm-wide horizontal band in the nasal-temporal direction containing the visual streak was cut from the center of the eye (Figure 4A) and fixed in 4% paraformaldehyde for 24 h. Thereafter, the tissue was embedded in optimal cutting medium and processed as described for mouse tissue.

Quantitative western blot analyses

Proteins were extracted as follows: enucleated mouse eyes were dissected in cold PBS buffer. Dissected retinas were flash-frozen immediately, and once all of the samples were collected, radioimmunoprecipitation assay buffer (catalog no. 89900, Thermo Scientific, Waltham, MA) with protease and phosphatase inhibitors (1:100 dilution; catalog no. 1861281, Thermo Scientific, Waltham, MA) was added and samples were homogenized by sonication. Samples were then centrifuged for 10 min at 4°C (13,000 rpm) and protein extracts were afterward transferred into a fresh tube. The protein concentration was quantified with the Bio-Rad protein assay (catalog nos. 5000113, 5000114, and 5000115, Bio-Rad, Hercules, CA). A total of 10 μg of protein were loaded per lane as previously described.[43] Sample sizes are as indicated in the figure legends. For pig eyes, the remainder of the retina was split into four quadrants based on the orientation. In each quadrant, a further incision was made to split the tissue into half, with one-half used for western blot analyses. Processing was performed as described for the mouse retina. All of the western blot quantifications were standardized to the β-actin signal of the control group. The antibodies used for protein detection were mouse anti-β-actin (1:1,000; catalog no. 3700, Cell Signaling Technology), rabbit anti-HTT (1:1,000; catalog no. 5656, Cell Signaling Technology), rabbit anti-PKCα (1:1,000; catalog no. 59754, Cell Signaling Technology), mouse anti-rhodopsin (1:1,000; catalog no. MA1-722, Invitrogen, Carlsbad, CA), rabbit anti-CA (1:1,000; catalog no. AB15282, Millipore), mouse anti-GS (1:1,000; catalog no. MAB302, Millipore), rabbit anti-Lim1 (1:1,000; catalog no. PA5-116485, Invitrogen), rabbit anti-VGAT (1:1,000; catalog no. PA5-27569, Invitrogen), and VGLUT2 (1:1,000; catalog no. 71555, Cell Signaling Technology). Protein detection was done using fluorescently labeled secondary (1:10,000) antibodies from LI-COR (Lincoln, NE) in combination with the Odyssey system. Quantification was performed with Image Studio software. The combination of these tools allows for optimal linear quantification independent of any postacquisition image modifications for visualization purposes.

Statistical analysis

Multiple t test was used for two-group comparisons (all statistics except Figure 3C) and two-way ANOVA was used for multiple group comparisons (Figure 3C). Two-tailed analyses were used in both analysis types. Significance levels are as follows: *$p < 0.05$; **$p < 0.01$; ***$p < 0.001$; and ****$p < 0.0001$. Specific analytic factors are mentioned in the corresponding figure legends.

DATA AND CODE AVAILABILITY

All of the data and experimental parameters related to this paper are available in the main text and the materials and methods section.

SUPPLEMENTAL INFORMATION

Supplemental information can be found online at https://doi.org/10.1016/j.omtn.2023.102088.

ACKNOWLEDGMENTS

This work was supported in part by a NEI grant (R01EY032461) and a pilot award from the UMass Center for Clinical and Translational Science, with funding from NCATS NIH (award no.UL1TR001453) to C.P. and an R35 GM131839 and S10 OD020012 to A.K. The authors thank Chih-Yun Cheng for the schematic drawings of the eTOC and Figure S1.

AUTHOR CONTRIBUTIONS

S.-Y.C., J.C., A.B., J.F.A., D.E., N.M., M.H., S.J., D.G., J.C., and C.P. performed the experiments and interpreted the data. S.-Y.C., J.F.A., A.K., and C.P. conceived the experiments and wrote the manuscript.

DECLARATION OF INTERESTS

A provisional patent application (63/412,051) describing the work and chemistry used in this study to treat eye disease has been submitted (Authors: C.P., A.K., M.H., J.F.A., A.B., S.-Y.C., J.C., and D. Moreno).

REFERENCES

1. Carthew, R.W., and Sontheimer, E.J. (2009). Origins and Mechanisms of miRNAs and siRNAs. Cell *136*, 642–655.
2. Ryther, R.C.C., Flynt, A.S., Phillips, J.A., 3rd, and Patton, J.G. (2005). siRNA therapeutics: big potential from small RNAs. Gene Ther. *12*, 5–11.
3. de Fougerolles, A., Vornlocher, H.P., Maraganore, J., and Lieberman, J. (2007). Interfering with disease: a progress report on siRNA-based therapeutics. Nat. Rev. Drug Discov. *6*, 443–453.
4. Hu, B., Zhong, L., Weng, Y., Peng, L., Huang, Y., Zhao, Y., and Liang, X.J. (2020). Therapeutic siRNA: state of the art. Signal Transduct. Target. Ther. *5*, 101.
5. Hassler, M.R., Turanov, A.A., Alterman, J.F., Haraszti, R.A., Coles, A.H., Osborn, M.F., Echeverria, D., Nikan, M., Salomon, W.E., Roux, L., et al. (2018). Comparison of partially and fully chemically-modified siRNA in conjugate-mediated delivery in vivo. Nucleic Acids Res. *46*, 2185–2196.
6. Li, J., Liu, J., Zhang, X., Clausen, V., Tran, C., Arciprete, M., Wang, Q., Rocca, C., Guan, L.H., Zhang, G., et al. (2021). Nonclinical Pharmacokinetics and Absorption, Distribution, Metabolism, and Excretion of Givosiran, the First

Approved N-Acetylgalactosamine-Conjugated RNA Interference Therapeutic. Drug Metab. Dispos. *49*, 572–580.

7. Janas, M.M., Zlatev, I., Liu, J., Jiang, Y., Barros, S.A., Sutherland, J.E., Davis, W.P., Liu, J., Brown, C.R., Liu, X., et al. (2019). Safety evaluation of 2'-deoxy-2'-fluoro nucleotides in GalNAc-siRNA conjugates. Nucleic Acids Res. *47*, 3306–3320.
8. Springer, A.D., and Dowdy, S.F. (2018). GalNAc-siRNA Conjugates: Leading the Way for Delivery of RNAi Therapeutics. Nucleic Acid Therapeut. *28*, 109–118.
9. Khvorova, A. (2017). Oligonucleotide Therapeutics - A New Class of Cholesterol-Lowering Drugs. N. Engl. J. Med. *376*, 4–7.
10. Fitzgerald, K., White, S., Borodovsky, A., Bettencourt, B.R., Strahs, A., Clausen, V., Wijngaard, P., Horton, J.D., Taubel, J., Brooks, A., et al. (2017). A Highly Durable RNAi Therapeutic Inhibitor of PCSK9. N. Engl. J. Med. *376*, 41–51.
11. Ahn, I., Kang, C.S., and Han, J. (2023). Where should siRNAs go: applicable organs for siRNA drugs. Exp. Mol. Med. *55*, 1283–1292.
12. Biscans, A., Haraszti, R.A., Echeverria, D., Miller, R., Didiot, M.C., Nikan, M., Roux, L., Aronin, N., and Khvorova, A. (2018). Hydrophobicity of Lipid-Conjugated siRNAs Predicts Productive Loading to Small Extracellular Vesicles. Mol. Ther. *26*, 1520–1528.
13. Alterman, J.F., Godinho, B.M.D.C., Hassler, M.R., Ferguson, C.M., Echeverria, D., Sapp, E., Haraszti, R.A., Coles, A.H., Conroy, F., Miller, R., et al. (2019). A divalent siRNA chemical scaffold for potent and sustained modulation of gene expression throughout the central nervous system. Nat. Biotechnol. *37*, 884–894.
14. Hariharan, V.N., Shin, M., Chang, C.W., O'Reilly, D., Biscans, A., Yamada, K., Guo, Z., Somasundaran, M., Tang, Q., Monopoli, K., et al. (2023). Divalent siRNAs are bioavailable in the lung and efficiently block SARS-CoV-2 infection. Proc. Natl. Acad. Sci. USA *120*, e2219523120.
15. Kaiser, P.K., Symons, R.C.A., Shah, S.M., Quinlan, E.J., Tabandeh, H., Do, D.V., Reisen, G., Lockridge, J.A., Short, B., Guerciolini, R., et al. (2010). RNAi-based treatment for neovascular age-related macular degeneration by Sirna-027. Am. J. Ophthalmol. *150*, 33–39.e2.
16. Byrne, M., Tzekov, R., Wang, Y., Rodgers, A., Cardia, J., Ford, G., Holton, K., Pandarinathan, L., Lapierre, J., Stanney, W., et al. (2013). Novel hydrophobically modified asymmetric RNAi compounds (sd-rxRNA) demonstrate robust efficacy in the eye. J. Ocul. Pharmacol. Therapeut. *29*, 855–864.
17. Hartong, D.T., Berson, E.L., and Dryja, T.P. (2006). Retinitis pigmentosa. Lancet *368*, 1795–1809.
18. Daiger, S.P., Sullivan, L.S., and Bowne, S.J. (2013). Genes and mutations causing retinitis pigmentosa. Clin. Genet. *84*, 132–141.
19. Brown, K.M., Nair, J.K., Janas, M.M., Anglero-Rodriguez, Y.I., Dang, L.T.H., Peng, H., Theile, C.S., Castellanos-Rizaldos, E., Brown, C., Foster, D., et al. (2022). Expanding RNAi therapeutics to extrahepatic tissues with lipophilic conjugates. Nat. Biotechnol. *40*, 1500–1508.
20. Alterman, J.F., Hall, L.M., Coles, A.H., Hassler, M.R., Didiot, M.C., Chase, K., Abraham, J., Sottosanti, E., Johnson, E., Sapp, E., et al. (2015). Hydrophobically Modified siRNAs Silence Huntingtin mRNA in Primary Neurons and Mouse Brain. Mol. Ther. Nucleic Acids *4*, e266.
21. Nikan, M., Osborn, M.F., Coles, A.H., Godinho, B.M., Hall, L.M., Haraszti, R.A., Hassler, M.R., Echeverria, D., Aronin, N., and Khvorova, A. (2016). Docosahexaenoic Acid Conjugation Enhances Distribution and Safety of siRNA upon Local Administration in Mouse Brain. Mol. Ther. Nucleic Acids *5*, e344.
22. Biscans, A., Coles, A., Haraszti, R., Echeverria, D., Hassler, M., Osborn, M., and Khvorova, A. (2019). Diverse lipid conjugates for functional extra-hepatic siRNA delivery in vivo. Nucleic Acids Res. *47*, 1082–1096.
23. Biscans, A., Coles, A., Echeverria, D., and Khvorova, A. (2019). The valency of fatty acid conjugates impacts siRNA pharmacokinetics, distribution, and efficacy in vivo. J. Contr. Release *302*, 116–125.
24. Ly, S., Navaroli, D.M., Didiot, M.C., Cardia, J., Pandarinathan, L., Alterman, J.F., Fogarty, K., Standley, C., Lifshitz, L.M., Bellve, K.D., et al. (2017). Visualization of self-delivering hydrophobically modified siRNA cellular internalization. Nucleic Acids Res. *45*, 15–25.
25. Biscans, A., Caiazzi, J., McHugh, N., Hariharan, V., Muhuri, M., and Khvorova, A. (2021). Docosanoic acid conjugation to siRNA enables functional and safe delivery to skeletal and cardiac muscles. Mol. Ther. *29*, 1382–1394.
26. Poché, R.A., Kwan, K.M., Raven, M.A., Furuta, Y., Reese, B.E., and Behringer, R.R. (2007). Lim1 is essential for the correct laminar positioning of retinal horizontal cells. J. Neurosci. *27*, 14099–14107.
27. Ruether, K., Feigenspan, A., Pirngruber, J., Leitges, M., Baehr, W., and Strauss, O. (2010). PKCalpha is essential for the proper activation and termination of rod bipolar cell response. Invest. Ophthalmol. Vis. Sci. *51*, 6051–6058.
28. Cueva, J.G., Haverkamp, S., Reimer, R.J., Edwards, R., Wässle, H., and Brecha, N.C. (2002). Vesicular gamma-aminobutyric acid transporter expression in amacrine and horizontal cells. J. Comp. Neurol. *445*, 227–237.
29. Johnson, J., Tian, N., Caywood, M.S., Reimer, R.J., Edwards, R.H., and Copenhagen, D.R. (2003). Vesicular neurotransmitter transporter expression in developing postnatal rodent retina: GABA and glycine precede glutamate. J. Neurosci. *23*, 518–529.
30. Luna, G., Keeley, P.W., Reese, B.E., Linberg, K.A., Lewis, G.P., and Fisher, S.K. (2016). Astrocyte structural reactivity and plasticity in models of retinal detachment. Exp. Eye Res. *150*, 4–21.
31. Sanchez, I., Martin, R., Ussa, F., and Fernandez-Bueno, I. (2011). The parameters of the porcine eyeball. Graefes Arch. Clin. Exp. Ophthalmol. *249*, 475–482.
32. Godinho, B.M.D.C., Gilbert, J.W., Haraszti, R.A., Coles, A.H., Biscans, A., Roux, L., Nikan, M., Echeverria, D., Hassler, M., and Khvorova, A. (2017). Pharmacokinetic Profiling of Conjugated Therapeutic Oligonucleotides: A High-Throughput Method Based Upon Serial Blood Microsampling Coupled to Peptide Nucleic Acid Hybridization Assay. Nucleic Acid Therapeut. *27*, 323–334.
33. Kovach, J.L., Schwartz, S.G., Flynn, H.W., Jr., and Scott, I.U. (2012). Anti-VEGF Treatment Strategies for Wet AMD. J. Ophthalmol. *2012*, 786870.
34. Gupta, A., Kafetzis, K.N., Tagalakis, A.D., and Yu-Wai-Man, C. (2021). RNA therapeutics in ophthalmology - translation to clinical trials. Exp. Eye Res. *205*, 108482.
35. Guzman-Aranguez, A., Loma, P., and Pintor, J. (2013). Small-interfering RNAs (siRNAs) as a promising tool for ocular therapy. Br. J. Pharmacol. *170*, 730–747.
36. Nguyen, Q.D., Schachar, R.A., Nduaka, C.I., Sperling, M., Basile, A.S., Klamerus, K.J., Chi-Burris, K., Yan, E., Paggiarino, D.A., Rosenblatt, I., et al. (2012). Phase 1 dose-escalation study of a siRNA targeting the RTP801 gene in age-related macular degeneration patients. Eye *26*, 1099–1105.
37. Nguyen, Q.D., Schachar, R.A., Nduaka, C.I., Sperling, M., Basile, A.S., Klamerus, K.J., Chi-Burris, K., Yan, E., Paggiarino, D.A., Rosenblatt, I., et al. (2012). Dose-ranging evaluation of intravitreal siRNA PF-04523655 for diabetic macular edema (the DEGAS study). Invest. Ophthalmol. Vis. Sci. *53*, 7666–7674.
38. Penn, J.S., Madan, A., Caldwell, R.B., Bartoli, M., Caldwell, R.W., and Hartnett, M.E. (2008). Vascular endothelial growth factor in eye disease. Prog. Retin. Eye Res. *27*, 331–371.
39. Nozaki, M., Raisler, B.J., Sakurai, E., Sarma, J.V., Barnum, S.R., Lambris, J.D., Chen, Y., Zhang, K., Ambati, B.K., Baffi, J.Z., and Ambati, J. (2006). Drusen complement components C3a and C5a promote choroidal neovascularization. Proc. Natl. Acad. Sci. USA *103*, 2328–2333.
40. Liao, D.S., Metlapally, R., and Joshi, P. (2022). Pegcetacoplan treatment for geographic atrophy due to age-related macular degeneration: a plain language summary of the FILLY study. Immunotherapy *14*, 995–1006.
41. O'Shea, J., Theile, C.S., Das, R., Babu, I.R., Charisse, K., Manoharan, M., Maier, M.A., and Zlatev, I. (2018). An efficient deprotection method for 5′-[O,O-bis(pivaloyloxymethyl)]-(E)-vinylphosphonate containing oligonucleotides. Tetrahedron *74*, 6182–6186.
42. Cheng, S.Y., Luo, Y., Malachi, A., Ko, J., Su, Q., Xie, J., Tian, B., Lin, H., Ke, X., Zheng, Q., et al. (2021). Low-Dose Recombinant Adeno-Associated Virus-Mediated Inhibition of Vascular Endothelial Growth Factor Can Treat Neovascular Pathologies Without Inducing Retinal Vasculitis. Hum. Gene Ther. *32*, 649–666.
43. Cheng, S.Y., Cipi, J., Ma, S., Hafler, B.P., Kanadia, R.N., Brush, R.S., Agbaga, M.P., and Punzo, C. (2020). Altered photoreceptor metabolism in mouse causes late stage age-related macular degeneration-like pathologies. Proc. Natl. Acad. Sci. USA *117*, 13094–13104.

OMTN, Volume *35*

Supplemental information

Single intravitreal administration of a tetravalent siRNA exhibits robust and efficient gene silencing in mouse and pig photoreceptors

Shun-Yun Cheng, Jillian Caiazzi, Annabelle Biscans, Julia F. Alterman, Dimas Echeverria, Nicholas McHugh, Matthew Hassler, Samson Jolly, Delaney Giguere, Joris Cipi, Anastasia Khvorova, and Claudio Punzo

Supplemental Figures

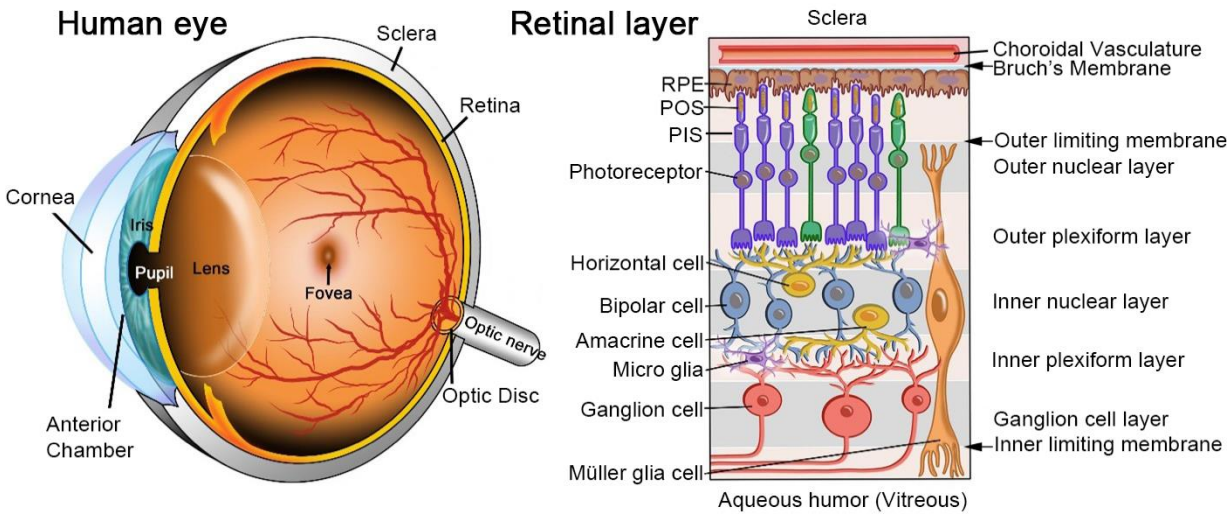

Figure S1. Schematic of eye and retina. Left panel: Schematic of a human eye showing the cornea, the anterior chamber, which is the space between the cornea and the iris, the pupil, the lens, the retina with the fovea, which is the area of high acuity vision in humans, the optic disc and the optic nerve, and the tissue holding the eye together, the sclera. Right panel: Schematic of a retinal cross-section showing the different cell layers and cell types. Width of individual layers are not to actual proportions. The Müller glia cells, span the retina, have the nucleus in the inner nuclear layer and form with their end-feet the inner and outer limiting membranes. Ganglion cells are in the ganglion cell layer and project their axons through the optic nerve to the brain. All interneurons are in the inner nuclear layer, including amacrine cells, horizontal cells, and bipolar cells. Amacrine and bipolar cells connect to ganglion cells in the inner plexiform layer while horizontal cells and bipolar cells connect to photoreceptors in the outer plexiform layer. Photoreceptors have their cell bodies in the outer nuclear layer. The photoreceptor inner segment (PIS) is on the outer side of the outer limiting membrane and contains all the major cytoplasmic components of the cell. The photoreceptor outer segment (POS) is connected to the PIS by the connecting cilium. The POS is the region where light photons are absorbed. POSs are surrounded by apical microvilli processes of the retinal pigmented epithelium (RPE). The RPE digests every day ~10% of each POS. RPE cells are attached to a basal membrane referred to as the Bruch's membrane. On the other side of the Bruch's membrane is the choroidal vasculature and the sclera. The siRNA that is injected intravitreally migrates across the inner limiting membrane and the retinal cell layers to the photoreceptors and the RPE cells. Very little remains in the vitreous or migrates to the lens and cornea.

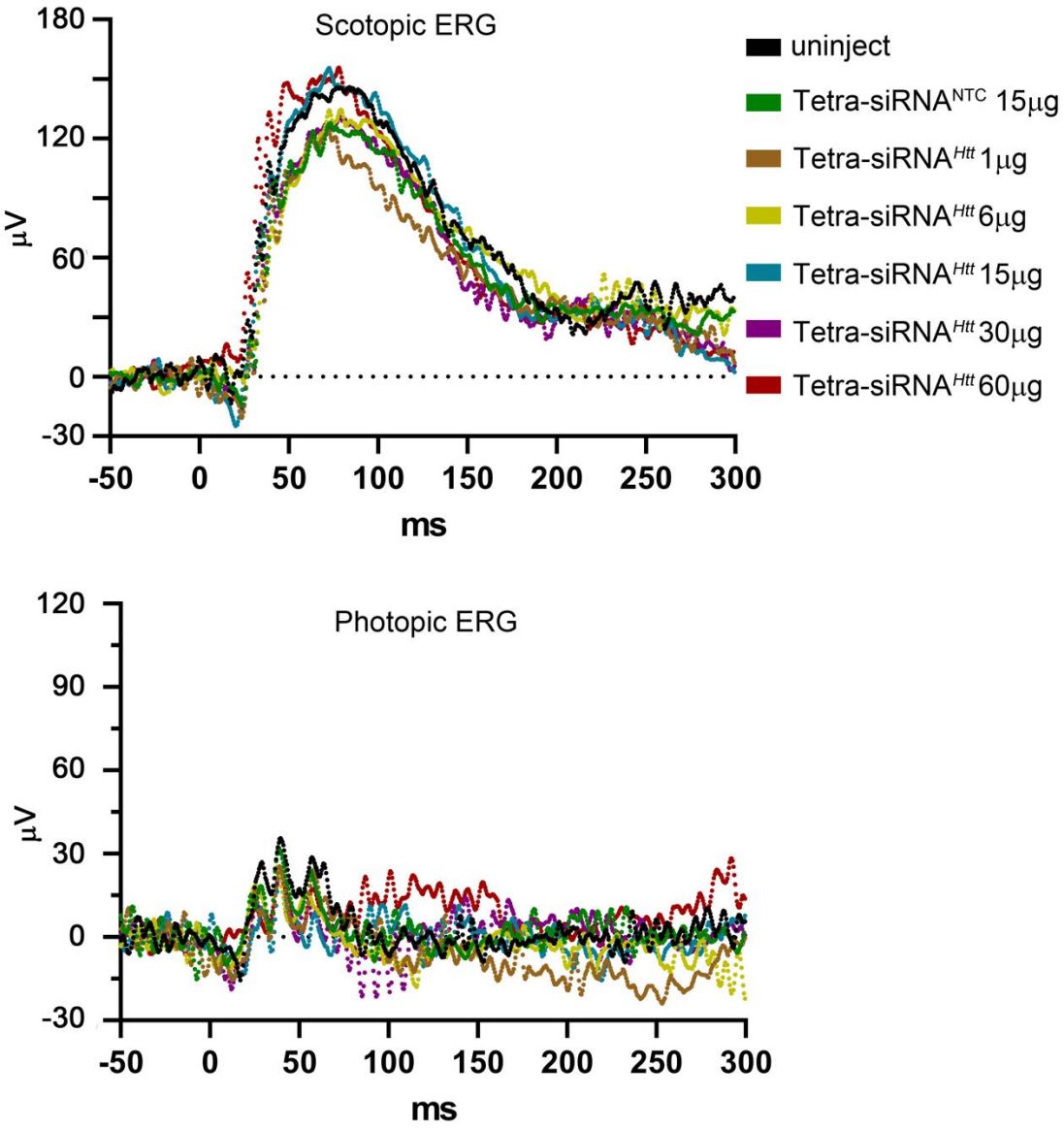

Figure S2. Electroretinogram wave forms. ERG wave forms for the scotopic (rod response, upper graph) and photopic (cone response, lower graph) ERG recordings performed 2 months post intravitreal injection with the different doses of the tetra-siRNA^{Htt}. Shown is one example per dose. The averages of the recordings are shown in Figure 3C. Scotopic recordings were performed at 1 cd.s/m^2. Photopic ERG recordings used a background intensity of 9cd.s/m^2 and a flash intensity of 10 cd.s/m^2.

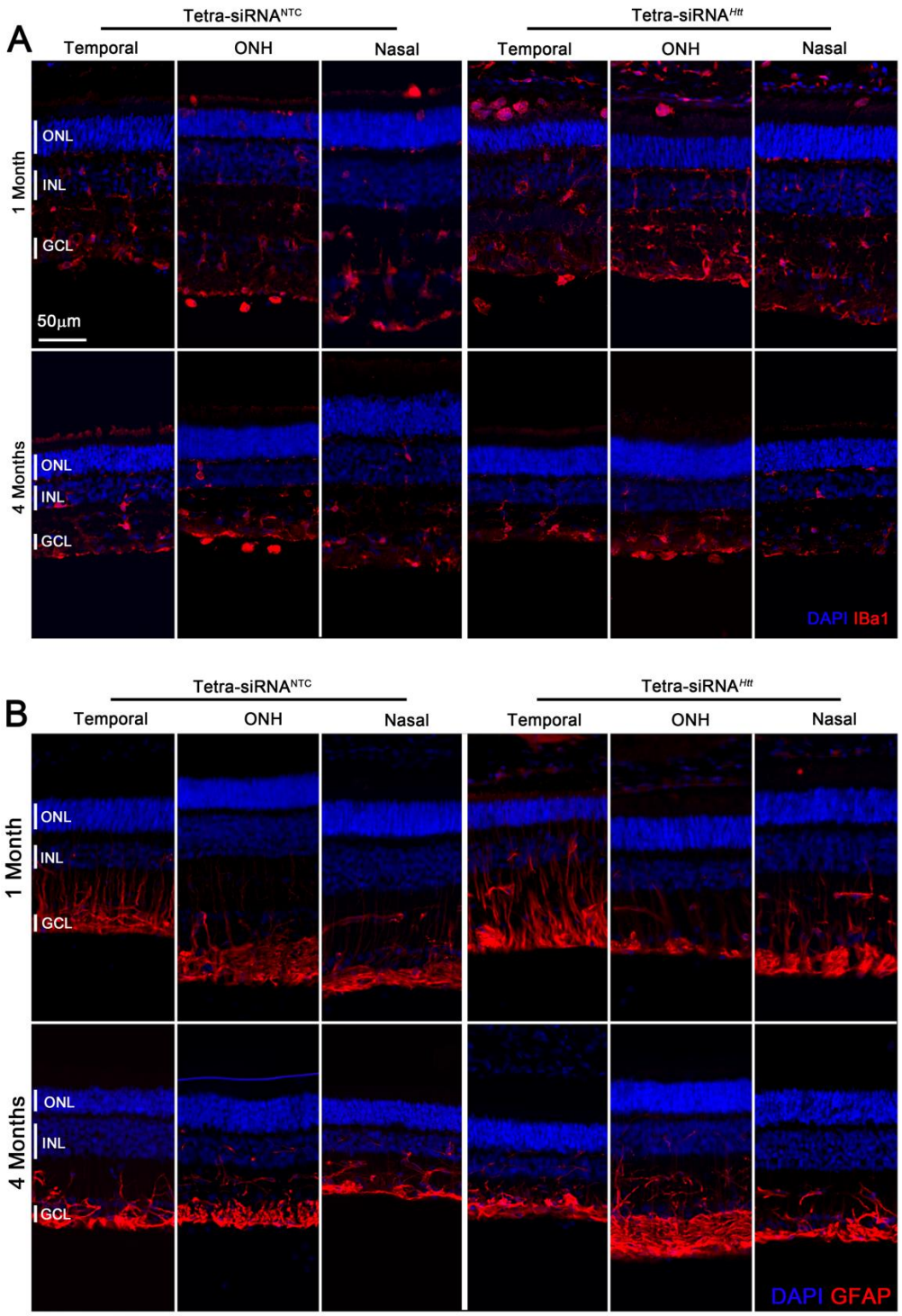

Figure S3. Safety of HTT silencing in porcine retina. (A and B) Retinal cross-sections stained for Iba1 (A: red signal) or GFAP (B: red signal) at 1-, and 4-months post intravitreal injection with 300µg of siRNA. The temporal side, where siRNA was injected shows slightly higher microglia activity and GFAP upregulation at 1-month post-injection. By 4-months post-injection microglia activity and GFAP expression appear normal again. Blue: nuclei marked with DAPI; red: Iba1 signal in (A) and GFAP signal in (B); ONL: outer nuclear layer; INL: inner nuclear layer; GCL: ganglion cell layer. Scale bar: 50µm. Images are representative images from 3 pigs per time point and siRNA.